MATERIALS SCIENCE

Bioinspired spring origami

Jakob A. Faber,[1] Andres F. Arrieta,[2]* André R. Studart[1]*

Origami enables folding of objects into a variety of shapes in arts, engineering, and biological systems. In contrast to well-known paper-folded objects, the wing of the earwig has an exquisite natural folding system that cannot be sufficiently described by current origami models. Such an unusual biological system displays incompatible folding patterns, remains open by a bistable locking mechanism during flight, and self-folds rapidly without muscular actuation. We show that these notable functionalities arise from the protein-rich joints of the earwig wing, which work as extensional and rotational springs between facets. Inspired by this biological wing, we establish a spring origami model that broadens the folding design space of traditional origami and allows for the fabrication of precisely tunable, four-dimensional–printed objects with programmable bioinspired morphing functionalities.

Programmable matter that can self-shape, morph, and actuate through "instructions" embedded into its own material architecture is widespread in nature and has opened exciting possibilities in robotics, biomedical technologies, arts, and design (*1*–*3*). Origami is particularly attractive because it allows folding simple, two-dimensional (2D) sheets into complex, 3D geometries. This simplicity and effectiveness of folding has inspired mathematicians, engineers, and materials scientists to exploit origami (*4*, *5*) as programmable metamaterials (*6*, *7*), reconfigurable structures (*8*–*10*), adaptive architectures (*11*, *12*), and soft robotic parts (*13*, *14*).

Despite its exciting prospects, major drawbacks remain when using classic origami principles. Classic origami, or rigid origami, uses two building blocks: rigid, planar facets of zero thickness and distinct, straight-line creases. These rigidity assumptions lead, in theory, to a limited design space of possible folding patterns (*15*). Besides these pattern constraints, a second aspect that limits functionality is that rigid origami mechanisms have only one degree of freedom, which is not associated with any stiffness during folding or unfolding. This lack of stiffness renders the resulting mechanisms purely kinematic (only describing motions) and thus hinders many engineering applications, particularly those involving load-bearing functions.

Attempts to extend the purely kinematic rigid origami principles have mainly been pursued by introducing bending energy in the creases (*5*, *16*). The addition of bending energy in the form of stiffness to the crease allows for forces and moments to be linked to the folding process; however, the design space for folding patterns remains unchanged. To account for additional folding patterns and programmability observed in practice on thin sheets, facet bending or twisting has been identified as an extra degree of freedom (*17*, *18*).

Despite these efforts, synthetic origami structures developed so far are still far from reaching the range of functionalities and design freedom observed in nature. An impressive natural example of folding pattern and functionality is the wings of Dermaptera, an order of insects commonly known as earwigs (Fig. 1A). The folding ratio (closed/open area) of these highly specialized wings is among the highest in the animal kingdom, with reported values of 1:10 (*19*) to 1:18 (*20*). This exceptionally high ratio concurrently allows for a large wing area during flight and a short, folded package to navigate the earwig's tight underground habitat (*21*). There are three very distinct features separating the wing-folding mechanism of Dermaptera from the assumptions of rigid origami. First, the earwig wing employs a pattern (Fig. 1B) that is incompatible with rigid origami theory because of angle mismatches and curved creases (*22*). Second, the wing has evolved to fully and rapidly self-fold from the open toward the closed state. The self-folding is achieved without the use of muscles. Instead, it

[1]Complex Materials, Department of Materials, ETH Zürich, 8093 Zürich, Switzerland. [2]Programmable Structures Lab, School of Mechanical Engineering, Purdue University, West Lafayette, IN 47907, USA.
*Corresponding author. Email: andre.studart@mat.ethz.ch (A.R.S.); aarrieta@purdue.edu (A.F.A.)

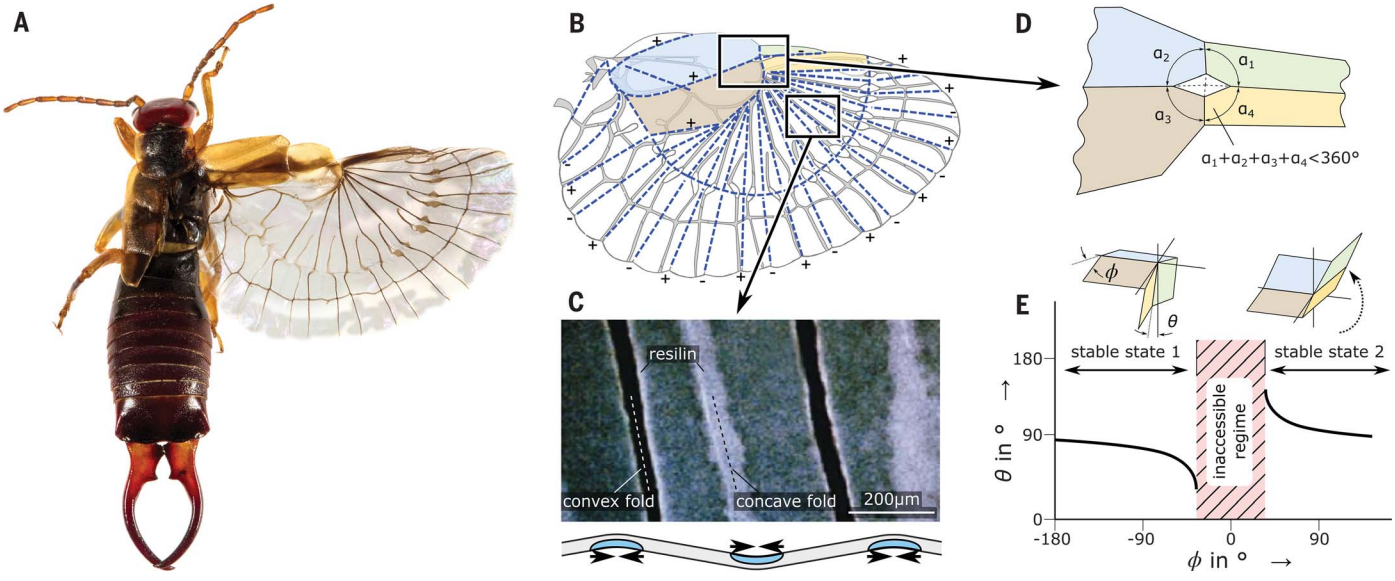

Fig. 1. Earwig wing as a natural example of multifunctional programmable folding. (**A**) The earwig *Forficula auricularia* with unfolded wing. [Image reprinted with permission from G. Wizen] (**B**) The folding pattern is incompatible with rigid origami assumptions. [Image adapted from Haas *et al*. (*19*)] (**C**) Alternating, asymmetric resilin distribution throughout the wing drives the self-folding process. The schematic under the microscopic image indicates the resilin-rich regions (in blue) along the cross-section of the wing. [Microscope image reprinted from (*19*) with permission by Elsevier] (**D**) Bistable central mechanism and angle mismatch. [Image adapted from Haas *et al*. (*19*)] (**E**) The inaccessible regime is responsible for the bistable function, but not accessible by origami kinematics. [Graph adapted from Haas (*23*) for a missing angle of 60°]

is preprogrammed in asymmetrically arranged, prestrained resilin in the joints (*19*) (Fig. 1C). Finally, a bistable snap-through mechanism (Fig. 1D) is incorporated in the structure to keep the unfolded wing in its open state. The open, locked state is stable enough to resist the aerodynamic loads during flight. The rigid origami model of this mechanism describes angular motions near the stable states (Fig. 1E), but exhibits a "forbidden range" (*23*) or inaccessible regime. Notably, this regime near the snap-through angle determines all functionality of the earwig wing. Thus, although the morphing of the earwig wing arises solely from the folding pattern and crease design, current origami models are not sufficient to describe its exceptional functionality even if bending facets are considered.

Our aim in this study is to identify design principles of the earwig wing and implement them in synthetic structures with pronounced stiffness and fast-morphing programmability. Therefore, we first investigate the earwig wing's self-folding behavior by finite element analysis (FEA) and derive the underlying principles embedded in the design of its natural joints. We then simplify the identified joint design using analogous mechanical springs. Using the newly introduced spring elements, we build a model of the wing's core mechanism to quantify its bistability and self-folding functions. Finally, these functions are transferred into 4D-printed, synthetic folding systems with unmatched and tunable functionality inspired by the natural example.

The self-folding and locking capability of the earwig wing relies on the presence of resilin-based joints. Resilin is an elastic biopolymer commonly linked to energy storage in natural systems, which has been found in symmetrical as well as asymmetrical arrangements in the earwig wing's joints (*19*). This through-thickness distribution of resilin in the joints determines the spring type: A symmetric distribution corresponds to an extensional spring, whereas an asymmetric distribution corresponds to a rotational spring. Combinations of both forms are possible. Whereas rotational springs have been discussed elsewhere (*5*, *16*), we now describe the role and resulting design capabilities of extensional springs for extending the pattern design space and generating locking, multistable folding systems.

To exploit the effect of the proposed extensional springs on the wing's self-folding behavior, we conducted folding simulations assuming either strict origami or spring-modified origami conditions (Fig. 2). Our results show that the geometrically incompatible folding pattern of the wing prevents complete folding if the strict conditions of traditional origami are considered (Fig. 2C). By contrast, full closure of the wing following the same pattern as the natural example is observed if the joints are treated as extensional and rotational springs. More details of these FEA simulations are provided in the supplementary materials. To assess the feasibility of this simulation, we produced a replica of the wing pattern by multimaterial 4D printing of stiff polymer facets (acrylonitrile butadiene styrene, ABS) and rubber-like hinges (thermoplastic polyurethane, TPU). The manually folded package confirms the stacking order and shape of the simulation results (Fig. 2D).

Despite the complexity of the simulated biological example and therefore the rather qualitative nature of these results, such proof-of-concept computational analysis clearly hints at the crucial role of membrane extensibility in making previously incompatible fold designs accessible.

The extensibility of joints not only facilitates the folding of complex patterns, but also paves the way to understand and synthetically design bioinspired features that were previously out of reach. The most notable feature of the earwig wing is its central mid-wing mechanism. It is bistable with two possible states: During folding, it is a classic Miura-Ori pattern with three convex and one concave fold. After fully opening and passing through an unstable flat state, it becomes a concave pyramid (Fig. 3A). In this shape, the mid-wing mechanism maintains the wing in its open flying configuration. Although it consists of only four facets, this crucial part of the wing simultaneously exhibits the mentioned features of interest; namely, self-folding, self-locking (bistability), and imperfect-pattern tolerance. Thus, a fundamental investigation of the interplay between membrane (extensional) and bending (rotational) elastic energy stored in folds of the mid-wing region provides valuable insights into the design principles of this morphing structure. To analytically model this four-facet unit cell, we use simple rotational and extensional springs (Fig. 3). The four rigid facets are interconnected by rotational and extensional springs at each joint (Fig. 3A). The spring constants of possible materials and geometries can easily be retrieved from the formulas given in the supplementary

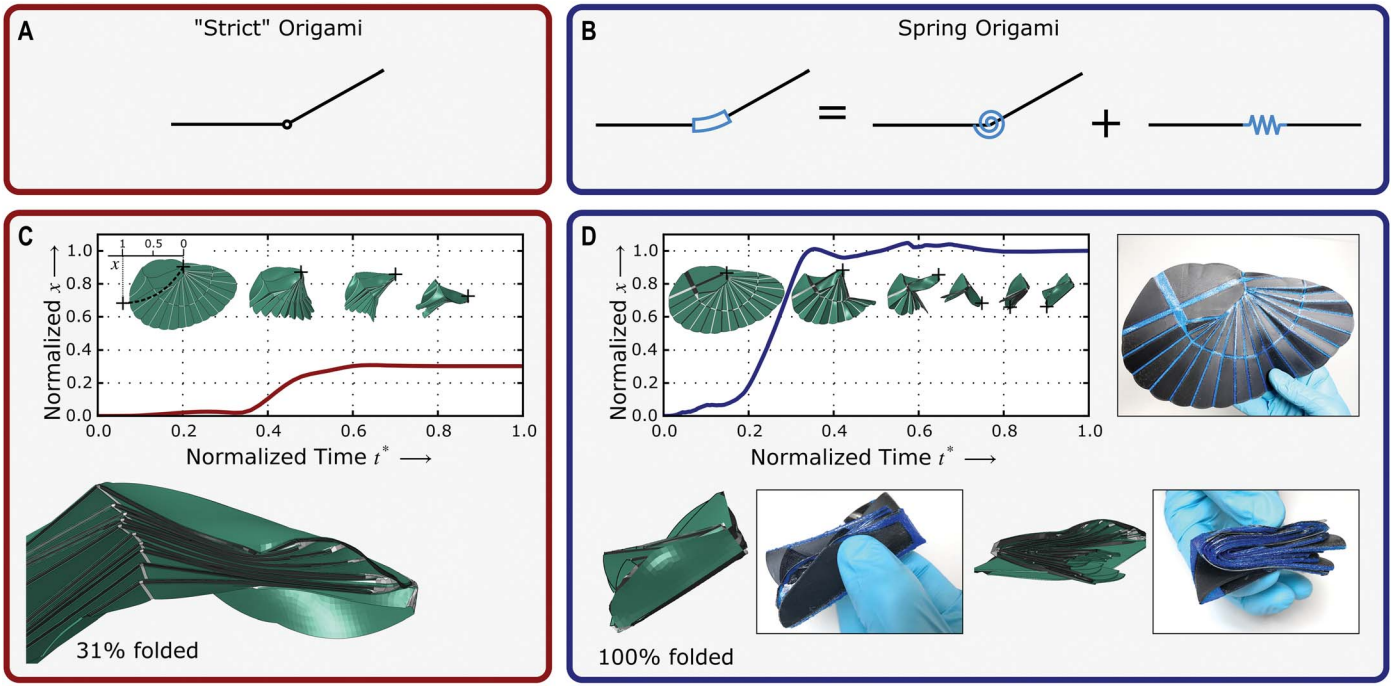

Fig. 2. Assumptions and FEA simulations describing the self-folding behavior of the earwig wing. (**A**) Strict (rigid) origami model. (**B**) Proposed interpretation of resilin occurrence as extensional and rotational spring elements. (**C**) Origami-inspired simulation approach leads to incomplete self-folding, whereas (**D**) the incorporation of spring elements in the origami structure results in complete self-folding of the simulated wing (movie S1). A multimaterial printed wing model confirms the shape and fold order of the simulated folded package.

materials. The energy stored in one rotational spring equals $\frac{1}{2}c_B(\Delta\phi)^2$, where c_B is the rotational spring stiffness and $\Delta\phi$ is the difference between the interfacet angle ϕ and the angle under which no bending stress occurs, $\phi_{0,B}$ (Fig. 3B). Similarly, the extensional spring energy is $\frac{1}{2}c_M(\Delta x)^2$, where c_M is the extensional spring stiffness and Δx is the spring extension x compared to its stress-free state $x_{0,M}$. Simple trigonometry links the spring extension x and the folding parameter ϕ (see Eq. S3), allowing for a convenient description of all energies in terms of ϕ (Fig. 3C). The extension-free angle obtained, $\phi_{0,M}$, is determined by the missing angle between the facets (see Eq. S10).

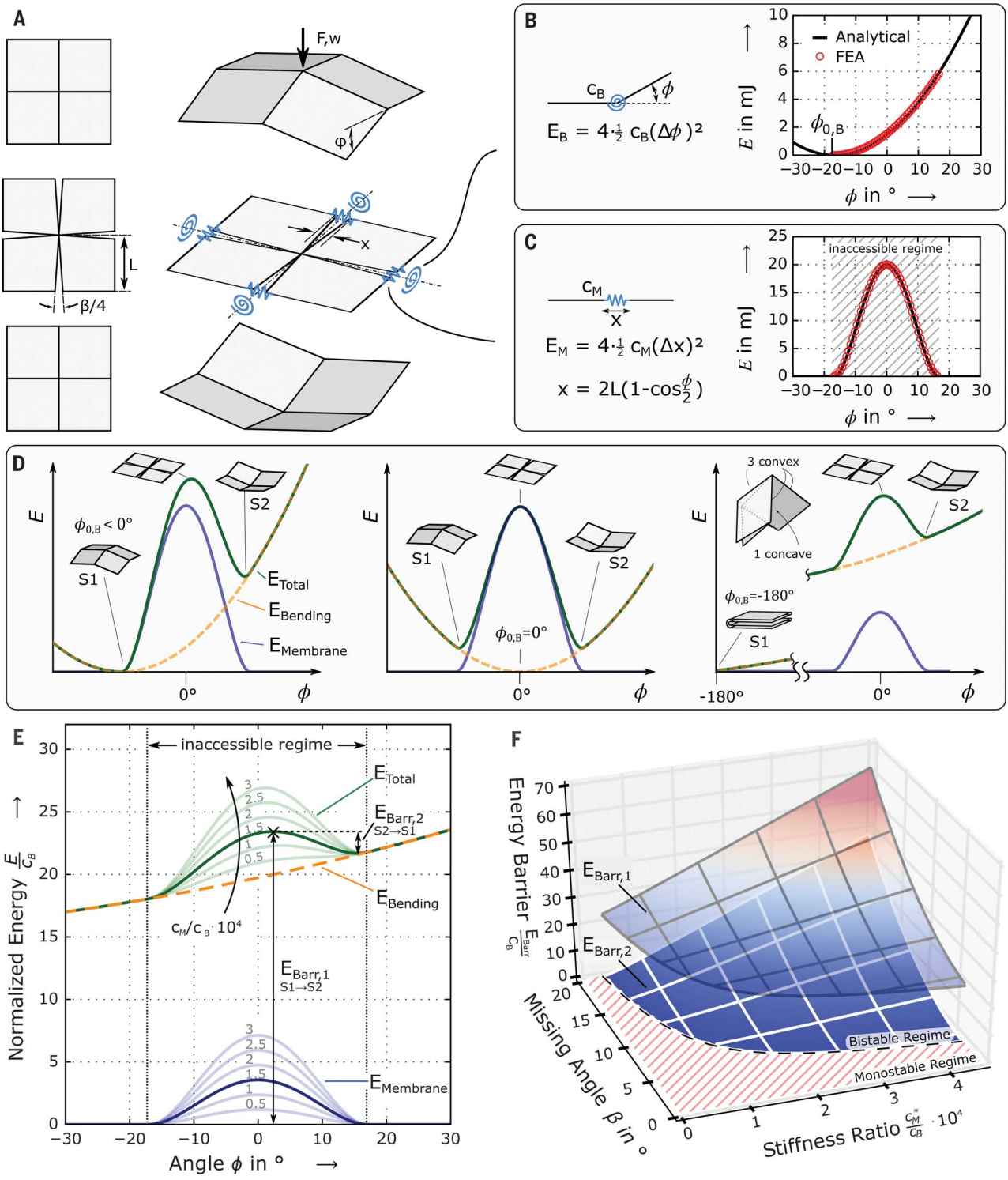

Fig. 3. Generalized model of bistable four-fold spring origami structures. (**A**) Geometry and spring arrangement. Analytical (**B**) rotational and (**C**) extensional spring energies and corresponding FEA evaluations. (**D**) Possible configurations and associated energy landscapes of selected four-faced spring origami structures. (**E**) Influence of the extensional spring stiffness on the energy landscape for β = 5° and definition of energy barriers. (**F**) Design map illustrating the effect of the missing angle and stiffness ratio on the magnitude of the energy barriers $E_{Barr,1}$ and $E_{Barr,2}$.

By computing the rotational and extensional contributions of the total energy stored in the joints of the mid-wing region, it is now possible to establish the energy landscape of the four-facet structure in different configurations (see assumptions in supplementary materials). In the inaccessible regime, the missing angle β must be compensated for by membrane extension, giving rise to an energy peak (Fig. 3, C and D). The rotational and extensional energy contributions can then be combined in endless configurations, depending on the folding patterns, each joint's stiffness values, and the programming parameters $\phi_{0,B}$ and $\phi_{0,M}$. Three exemplary configurations are shown in Fig. 3D. The initially

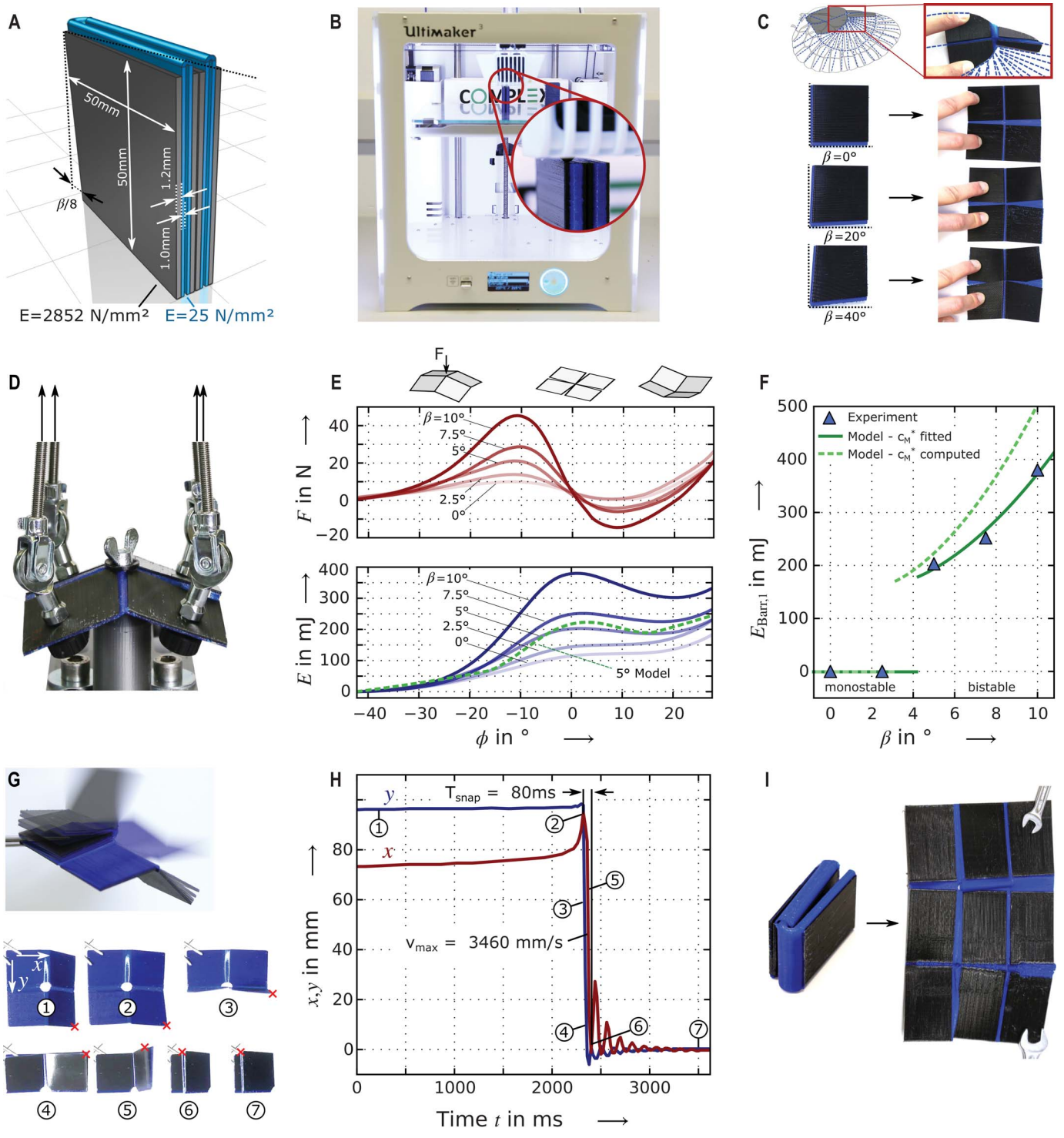

Fig. 4. Four-dimensional printing and experimental investigation of spring origami mechanisms. (**A**) Geometry and material properties. (**B**) FDM printing in the folded, upright state. (**C**) Nondevelopable, 4D-printed designs using the earwig wing's central mechanism contours (top) and simplified rectangular facet contours with different missing angles. (**D**) Cardan test rig. (**E**) Measured forces and related energy plots for mechanisms with increasing missing angle β. Model prediction for β = 5° is shown by the dashed green curve. (**F**) Effect of the missing angle on the energy barrier magnitudes and model predictions. (**G** and **H**) Fast self-folding after slow internal stimulus (movie S1). (**I**) A 4D-printed, nondevelopable 3 × 3–panel array.

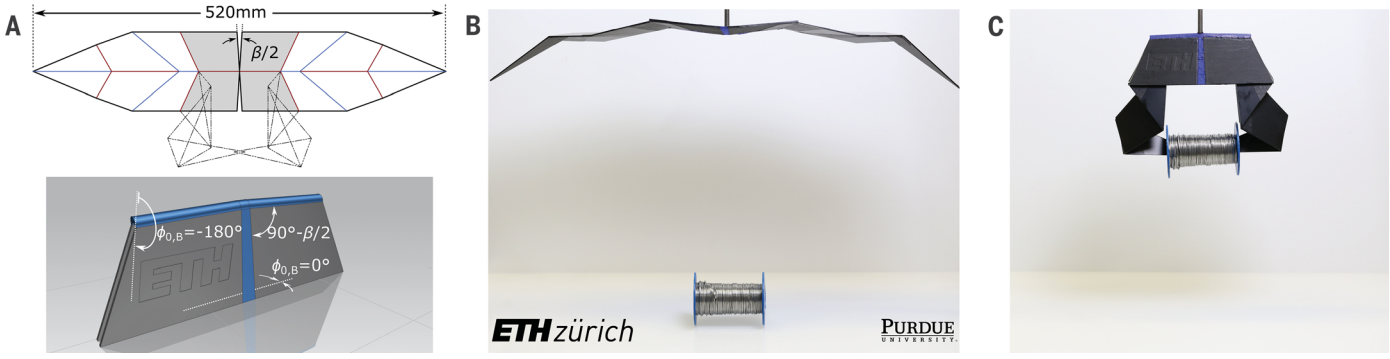

Fig. 5. Spring origami gripper (movie S2). (**A**) Fold pattern. Gray facets and computer-assisted design model: preprogrammed control cell. White facets: passive part of mechanism. (**B**) Stable state 1: open. (**C**) Stable state 2: closed. The closed state exerts force on the gripped object without constant actuation.

mentioned case of a stress-free "pyramid" as the base state leads to an asymmetrical energy landscape (Fig. 3D, left). A symmetrical case can be reached by planar assembly of facets, including a missing angle and using prestretched joint regions (Fig. 3D, center). Assembling three convex ($\phi_{0,B} = -\pi$) and one concave fold ($\phi_{0,B} = +\pi$), as in the case of the earwig wing, yields the exemplary Miura-Ori configuration, which serves as our base system. These preprogrammed angles lead to a fully folded pattern as the stress-free state (Fig. 3D, right).

For a technical application of the described unit cell, it is necessary to understand and model the relation between design parameters and resulting morphing and mechanical properties. Applying the basic building blocks from Fig. 3, A to D, we computed design maps of two kinds: First, Fig. 3E shows the bending, membrane, and total stored energies over ϕ for the self-folding Miura-Ori configuration, displaying a constant missing angle β. A low membrane stiffness ratio (c_M/c_B) leads to monostable systems resulting from the lack of an energy barrier that could give rise to two distinct mechanical states. These systems are bending-dominated and will return to their preprogrammed shape immediately. For stiffness ratios of $\frac{c_M}{c_B} > 0.5 \times 10^4$, a barrier develops in the energy landscape, leading to the two minima that characterize a bistable system. This threshold from mono- to bistability changes with the missing angle, which increases the energy barrier and therefore shifts the overall behavior toward more pronounced bistability. The combined effect of both stiffness values c_M and c_B, as well as the missing angle β, on the magnitude of the energy barriers $E_{Barr,1}$ and $E_{Barr,2}$ is shown in the design map depicted in Fig. 3F. E_{Barr} scales proportionally with c_M and c_B as long as their ratio is constant (see Eqs. S1 and S2). For each $\frac{c_M}{c_B}$ ratio, there is a critical missing angle β_c that makes the folding pattern bistable, and vice versa (Fig. 3F). The parameter space revealed by these maps allows us to determine appropriate variables to design folding behavior, stable states, and tuned energy barriers in spring origami systems. Such features control the direction and order of folding, the obtainable geometries, and the self-locking strength. Furthermore, the derivatives of the energy plots allow one to directly obtain folding moments and forces, which are relevant for the design of load-bearing functions in both stable states (see Eqs. S1 and S5). As is the case in the earwig wing, this unit cell can serve as an embedded control unit for much larger folding patterns and complex geometries. In the following section, we discuss how this Miura-Ori configuration can be exploited in exemplary synthetic systems to achieve fast folding and locking mechanisms with minimal actuation inspired by the earwig wing.

We transferred the biological design principles extracted from the earwig wing into a functional synthetic folding system that can be directly manufactured by 4D printing using a conventional additive manufacturing process (Fig. 4). The base configuration was a fourfold structure of 100 mm by 100 mm unfolded edge length with 1.2-mm-thick facets made of a stiff component [polylactic acid (PLA) or ABS] and joints made from an elastomeric component (TPU) with a thickness of 1.0 mm (Fig. 4A). Using multimaterial fused deposition modeling (FDM, Fig. 4B), we can overcome several limitations of conventional origami-type folding approaches. First, printing allows us to preprogram the folding pattern in an elegant way: Instead of using selective shrinking or swelling of a bilayer architecture to induce bending (*14*, *24*, *25*), we printed the samples in the fully folded configuration. This allows us to set $\phi_{0,B} = \pm\pi$ in the desired combination. If bistability is simultaneously required, simple folding techniques also fail. Any missing angle $\beta \neq 0$ renders the fold pattern nondevelopable, which means not foldable from a flat sheet. Our folded-printing approach allows us to program $\phi_{0,M}$ by directly implementing the missing angle β in the geometry. Figure 4C demonstrates the relationship between the printed and the unfolded geometry with the missing angle β ranging from 0° to 40°.

To illustrate the distinctive folding and mechanical functionalities of the printed spring origami, we measured the force required to keep the structure at a constant interfacet angle near and within the inaccessible region (Fig. 1E). The energy curves obtained through integration of the measured forces feature the two-well landscapes characteristic of bistable systems (Fig. 4E, blue curves). The experimental curves and the earlier model predictions match quantitatively very well the dependence of the stored energy on the folding angle (Fig. 4E, dashed line). The magnitude of the energy barrier observed in these curves rises in a progressive manner with increasing missing angles β and shows the predicted bistability threshold behavior (Fig. 4F). Small missing angles lead to the monostable systems predicted by our model (compare Fig. 3E), whereas bistability arises above the expected threshold.

Our ability to tune the energy barrier between bistable states using simple geometrical and material properties (Fig. 3F) enables the design and fabrication of spring origami structures that can undergo fast morphing, triggered by an environmental stimulus. As opposed to other common biological and synthetic morphing systems that react to external stimuli (*26*–*28*), the elastic energy stored in spring origami results in very fast intrinsic folding of the structure. Tracking the motion of a Miura-Ori structure during self-folding allowed us to quantify the dynamics of this fast morphing process (Fig. 4, G and H). The snap-through between the two stable states occurs in 80 ms, much faster than conventional diffusion-driven mechanisms. This is equivalent to the fast actuation mechanism used by the Venus flytrap or the underwater suction trap Utricularia, which also convert a slow stimulus to a rapid movement by bistability concepts (*29*, *30*).

We also demonstrate the scalability of our 4D-printing approach beyond four-facet systems by printing larger arrays (Fig. 4I), or by using a single spring origami element to control more complex structures that fold via conventional mechanisms. To illustrate this possibility, we fabricated a spring origami gripper that actuates with a low-energy input (Fig. 5 and movie S2). The gripper consists of a passive fold pattern (white) responsible for the kinematic gripping movement and a central, 4D-printed spring origami element (gray) that defines the energy landscape of the folding system. By designing the

materials and geometrical parameters (Fig. 5A) of this cell—namely, missing angle, stiffness values, and strain-free fold angles—the inherent energy landscape of the entire gripper mechanism can be programmed. Our spring origami gripper eventually displays the bistable and fast self-folding functionalities of the earwig wing. The programmed stable states (Fig. 5, B and C) and energy landscape allows the spring origami structure to exert a force on the gripped object without the need for constant external actuation. This contrasts with purely passive rigid origami mechanisms, which would yield to any applied load owing to the absence of an energy landscape or stable states. The spring origami gripper can thus remain in both the open (Fig. 5B) or closed positions (Fig. 5C) and lift objects of its own body weight.

Origami structures featuring extensional and rotational joints inspired by the earwig wing show unusual self-locking, fast-morphing, and geometry-tolerant folding patterns that are not allowed in conventional origami theory. The possibility of 4D printing 3D objects whose morphing and mechanical behavior are programmed with the material architecture brings us closer to the design strategies underlying the exquisite dynamics of biological self-shaping structures. The ample design space provided by the proposed spring origami systems can potentially be used to fabricate biomedical devices with patient-specific morphing features, collapsible portable displays, soft robots, or deployable spacecraft modules.

REFERENCES AND NOTES

1. I. Burgert, P. Fratzl, *Philos. Trans. A Math. Phys. Eng. Sci.* **367**, 1541–1557 (2009).
2. L. D. Zarzar, J. Aizenberg, *Acc. Chem. Res.* **47**, 530–539 (2014).
3. A. Ghadban *et al*., *Chem. Commun. (Camb.)* **52**, 697–700 (2016).
4. A. Lebée, *Int. J. Space Structures* **30**, 55–74 (2015).
5. N. Turner, B. Goodwine, M. Sen, *J. Mec.* **230**, 2345–2362 (2016).
6. J. L. Silverberg *et al*., *Science* **345**, 647–650 (2014).
7. S. Shan *et al*., *Adv. Funct. Mater.* **24**, 4935–4942 (2014).
8. E. A. Peraza-Hernandez, D. J. Hartl, R. J. Malak Jr., D. C. Lagoudas, *Smart Mater. Struct.* **23**, 094001 (2014).
9. S. Waitukaitis, R. Menaut, B. G. Chen, M. van Hecke, *Phys. Rev. Lett.* **114**, 055503 (2015).
10. S. Daynes, R. S. Trask, P. M. Weaver, *Smart Mater. Struct.* **23**, 125011 (2014).
11. S. Tibbits, K. Cheung, *Assem. Autom.* **32**, 216–225 (2012).
12. P. M. Reis, F. López Jiménez, J. Marthelot, *Proc. Natl. Acad. Sci. U.S.A.* **112**, 12234–12235 (2015).
13. J. Mu *et al*., *Sci. Adv.* **1**, e1500533 (2015).
14. S. Felton, M. Tolley, E. Demaine, D. Rus, R. Wood, *Science* **345**, 644–646 (2014).
15. T. Tachi, *Origami* **4**, 175–187 (2009).
16. V. Brunck, F. Lechenault, A. Reid, M. Adda-Bedia, *Phys. Rev. E* **93**, 033005 (2016).
17. F. Lechenault, M. Adda-Bedia, *Phys. Rev. Lett.* **115**, 235501 (2015).
18. J. L. Silverberg *et al*., *Nat. Mater.* **14**, 389–393 (2015).
19. F. Haas, S. Gorb, R. J. Wootton, *Arthropod Struct. Dev.* **29**, 137–146 (2000).
20. J. Deiters, W. Kowalczyk, T. Seidl, *Biol. Open* **5**, 638–644 (2016).
21. J. F. V. Vincent, in *Deployable Structures*, S. Pellegrino, Ed. (Springer Vienna, Vienna, 2001), pp. 37–50.
22. E. D. Demaine, J. O'Rourke, *Geometric Folding Algorithms: Linkages, Origami, Polyhedra* (Cambridge Univ. Press, Cambridge, 2007), pp. 292–296.
23. F. Haas, Geometry and mechanics of hind-wing folding in Dermaptera and Coleoptera, thesis, University of Exeter (1994).
24. Q. Ge, C. K. Dunn, H. J. Qi, M. L. Dunn, *Smart Mater. Struct.* **23**, 094007 (2014).
25. R. M. Erb, J. S. Sander, R. Grisch, A. R. Studart, *Nat. Commun.* **4**, 1712 (2013).
26. Y. Liu, J. K. Boyles, J. Genzer, M. D. Dickey, *Soft Matter* **8**, 1764–1769 (2012).
27. A. Lendlein, S. Kelch, *Angew. Chem. Int. Ed.* **41**, 2034–2057 (2002).
28. A. Papadopoulou *et al*., *Addit. Manuf.* **2**, 106–116 (2015).
29. Y. Forterre, J. M. Skotheim, J. Dumais, L. Mahadevan, *Nature* **433**, 421–425 (2005).
30. O. Vincent *et al*., *Proc. R. Soc. London Ser. B* **278**, 2909–2914 (2011).

ACKNOWLEDGMENTS

We especially thank K. Masania and S. Gantenbein for help with the 3D-printing experiments, M. Binelli for the gripper suggestion, E. Jeoffroy for help with photos and movies, and all colleagues for fruitful discussions. **Funding:** We are grateful for financial support from ETH Zürich, Purdue University, European Office of Aerospace Research and Development (grant FA9550-16-1-0007), and the Air Force Office of Scientific Research (grant FA9550-17-1-0074). **Authors contributions:** All authors designed the research. The analytical, numerical, and experimental work was designed, performed, and evaluated by J.A.F. The manuscript was prepared by J.A.F., A.R.S., and A.F.A. All authors discussed and critically assessed the results and their implications, and revised the manuscript at all stages. **Competing interests:** The authors declare no competing financial interests. **Data and materials availability:** All data are available in the manuscript or supplementary materials.

SUPPLEMENTARY MATERIALS

www.sciencemag.org/content/359/6382/1386/suppl/DC1
Materials and Methods
Figs. S1 and S2
Table S1
Movies S1 to S3
Python Code of Spring Origami Model
Raw Data of Mechanical Testing
Raw Data of Image Analysis
3D-Printing Files

25 August 2017; accepted 30 January 2018
10.1126/science.aap7753

Bioinspired spring origami

Jakob A. Faber, Andres F. Arrieta and André R. Studart

Science **359** (6382), 1386-1391.
DOI: 10.1126/science.aap7753

More than just simple folding

Origami involves folding two-dimensional sheets into complex three-dimensional objects. However, some shapes cannot be created using standard folds. Faber *et al.* studied the wing of an earwig, which can fold in ways not possible using origami and can alter its shape for flight. The authors replicated this ability by using a membrane that allows for deformations and variable stiffness. Prestretching generated energetically bistable origami patterns that exhibited passive self-folding behavior.

Science, this issue p. 1386